crystals

MDPI

Article

Dissolution Behavior of Al_2O_3 Inclusions in CaO-Al_2O_3 Based Slag Representing Aluminothermic Reduction Slag

Guan-Yong Shi [1,2], Ting-An Zhang [2,*], Zhi-He Dou [2] and Li-Ping Niu [2]

[1] Institute of Green Metallurgy and Process Intensification, Jiangxi University of Science and Technology, Ganzhou 341000, China; shigy@jxust.edu.cn

[2] Key Laboratory for Ecological Metallurgy of Multimetallic Ores (Ministry of Education), Northeastern University, Shenyang 110819, China; douzh@smm.neu.edu.cn (Z.-H.D.); niulp@smm.neu.edu.cn (L.-P.N.)

* Correspondence: zta2000@163.net; Tel.: +86-024-8368-7715

Received: 9 October 2020; Accepted: 20 November 2020; Published: 22 November 2020

Abstract: In the preparation of CuCr alloy using the self-propagating high-temperature synthesis (SHS)-metallurgy method, the dissolution of alumina in molten slag has an important influence in two key steps: aluminum thermal reduction and slag refining. In the present work, the dissolution behavior of Al_2O_3 into molten SHS-metallurgical slags was investigated by employing the rotating cylinder method and static dissolution method. It is concluded that the increase of MgO, CaF_2, CaO, and Na_3AlF_6 contents can increase the dissolution rate of alumina in SHS-metallurgical slag, and the order of influence is from strong to weak. Both temperature and rotating speed can increase the dissolution rate, and the rate-limiting step is the diffusion of alumina in the boundary layer, with the solid alumina first reacting with lime to form two intermediate phases, $CaO{\cdot}2Al_2O_3$ and $CaO{\cdot}6Al_2O_3$, and finally dissolving into the slag in the form of an aluminum polymer.

Keywords: Al_2O_3 dissolution behavior; aluminate slag; intermediate compounds

1. Introduction

Due to its superior properties, copper-chromium alloys are widely used as medium and high voltage vacuum switch contact materials in the modern power industry [1,2]. When using traditional self-propagating high-temperature synthesis (SHS) processes to prepare CuCr alloy, once the exothermic reaction ceases to be active, the metal and slag melt will solidify quickly. This will result in a large amount of alumina inclusions in the CuCr alloy [3,4]. Zhang et al. [5] invented a new method for the preparation of CuCr alloy using the self–propagation high–temperature synthesis (SHS)-metallurgy process. In this process, high temperature melts obtained by the aluminothermic reaction are transferred to an induction furnace. Therefore, the melt can be maintained at a high temperature for the slag refining process, during which the alumina inclusions in the metal melt can float up and dissolve into the slag. Finally, the alloy ingot is obtained by rapid cooling. During the thermite reaction process, a portion of the Al_2O_3 produced by the aluminothermic reaction combines with the slagging agent to form the initial molten slag, and then the remaining Al_2O_3 dissolves into the primary slag. Due to the violent flow of the melt, some of the alumina remains in the original alloy melt, then floats during the slag refining process and is adsorbed and dissolved by the slag. The residual Al_2O_3 floats and is adsorbed and dissolved by the slag during the slag refining process. Therefore, the investigation of the dissolution behavior of alumina inclusions in SHS-metallurgical slag is very significant.

In recent years, there has been a considerable amount of research on the dissolution of alumina in metallurgical slag including in silicate slag [6], mold fluxes [7,8], secondary steelmaking slags [9],

the CaO-Al_2O_3-Fe_2O_3 system [10], the Al_2O_3–CaO–FeO_x–SiO_2 system [11], and CaO-Al_2O_3-SiO_2 [12,13]. Existing studies on the dissolution of alumina in aluminate melts are not sufficient. Sridhar et al. [14] investigated the dissolution of Al_2O_3 and MgO inclusions in the CaO-Al_2O_3-MgO system using the confocal scanning laser microscope (CSLM) method. Chou et al. [15] investigated the dissolution of Al_2O_3 inclusions in the CaO-Al_2O_3-CaF_2 system using the rotating cylinder method. Dong et al. [16] investigated the dissolution of Al_2O_3 inclusions in CaF_2-Al_2O_3-CaO-MgO-SiO_2 ESR slag using optical microscopy (OM) and scanning electron microscopy (SEM) analysis of quenched slag. Sridhar's research did not find the formation of intermediate compounds at the alumina/slag interface and found that the dissolution process of alumina is controlled by diffusion [14]. Some investigators [13,15] suggested that alumina dissolution should be controlled by diffusion in the boundary layer.

In the preparation of CuCr alloy using the SHS-metallurgy method, the refining slag is formed by the combination of alumina produced by the aluminothermic reaction and slagging agent. When the content of the slag-forming agent is low, the viscosity and melting point of the slag are too high, and if the content is too high, the temperature of the aluminothermic reaction will decrease. Both of these cases are not conducive to the preparation process of the alloy. Therefore, the composition adjustment range of SHS-metallurgical slag is quite limited, and the slags are aluminate melts with high Al_2O_3 content. To the best knowledge of the present author, there is no study regarding Al_2O_3 dissolution in high Al_2O_3 content aluminate systems in the literature. In the present work, the dissolution behavior of Al_2O_3 in SHS-metallurgical slag was studied by the dynamic and static dissolution process of Al_2O_3 rods in slag.

2. Experimental Procedures

2.1. Experiment Materials and Equipment

The molten slags used in the experiments were synthesized by analytically pure reagents provided by Sinopharm Chemical Reagent Co. Ltd., Shanghai, China. In order to remove moisture and volatile impurities, all reagents are pretreated at high temperature in a muffle furnace. CaF_2 and Na_3AlF_6 were pretreated at 773 K (500 °C) for 6 h; CaO, MgO, and SiO_2 were pretreated at 1273 K (1000 °C) for 4 h. The alumina samples were high-purity corundum rods (>99.5 mass %) produced by Beijing Dingsheng Brother Technology Co., Ltd., Beijing, China.

The experiments were carried out with an RTW-10 melts properties analyzer (Designed and manufactured by Northeastern University, Shenyang, China), and its schematic diagram is shown in Figure 1. The heating process was carried out in a tube furnace with six u-type $MoSi_2$ heating elements and a high-purity corundum furnace tube. The heating zone of the tube furnace was 250 mm high and the constant temperature zone was 80 mm high. The temperature of the furnace was controlled within ±1 K with a B-type (PtRh30-PtRh6) thermocouple. The temperature measurement point was on the outside of the furnace tube and in the middle of the constant temperature zone. In order to improve the accuracy of temperature measurement of the melts, another B-type thermocouple was placed just under the crucible for the measurement of the temperature of the melts.

2.2. Experiment Methods

The research on the dynamic dissolution process of Al_2O_3 in slag was carried out using the rotating cylinder method. The various reagents were thoroughly mixed according to the predetermined composition ratio, and then 150 g of the powder mixture was accurately weighed. The mixture was heated and melted in the graphite crucible (outer diameter 49 mm, inner diameter 40 mm, length 80 mm) and then thermostated at the predetermined temperature for 1 h to ensure uniform melt composition. When the temperature reached 300 °C, high purity Ar gas was introduced into the furnace at a flow rate of 0.5 L/min until the temperature was lowered to below 500 °C after the end of the experiment. The Al_2O_3 rods (10 mm in diameter and 100 mm in length) were fixed by a molybdenum fixture and attached to the motor with variable rotation speed by a 4 mm diameter corundum rod. The Al_2O_3

rods were slowly placed into the furnace until the lower end of the sample was about 10 mm from the surface of the melt and held for 10 min to allow the sample to be fully heated. Then, the Al_2O_3 rod was immersed into the molten slag until the lower end of the sample was about 10 mm from the bottom of the crucible and rotated at the required speed. After the end of the experiment, the Al_2O_3 rods were quickly removed from the melt and then slowly transferred to the outside of the furnace to avoid cracking. Subsequently, the adhered slag on the surface of the Al_2O_3 rods was removed with hydrochloric acid. The mass and size of the Al_2O_3 rods were measured by electronic balance and vernier caliper before and after the experiment. The Al_2O_3 rods were treated in a muffle furnace at 1000 °C for one hour before measurement to remove moisture and volatile impurities. The dissolution rate of Al_2O_3 in the slag can be calculated as follows [17]:

$$R_d = \frac{\Delta m}{S \times t} \tag{1}$$

$$S = \pi \times h \times \frac{(d_1 + d_2)}{2} + \pi \times \frac{(d_1 + d_2)^2}{4} \tag{2}$$

where: R_d represents the Al_2O_3 dissolution rate of alumina in the slag ($g \cdot cm^{-2} \cdot s^{-1}$); Δm represents the weight loss of the corundum rods (g); t represents the rotation time (min); S represents the average contact area between the rod and the slag (cm^2); h represents the average height of contact between the corundum rod and the slag, cm; and d_1 and d_2 represent the average diameter of the corundum rod before and after the experiment (cm), respectively.

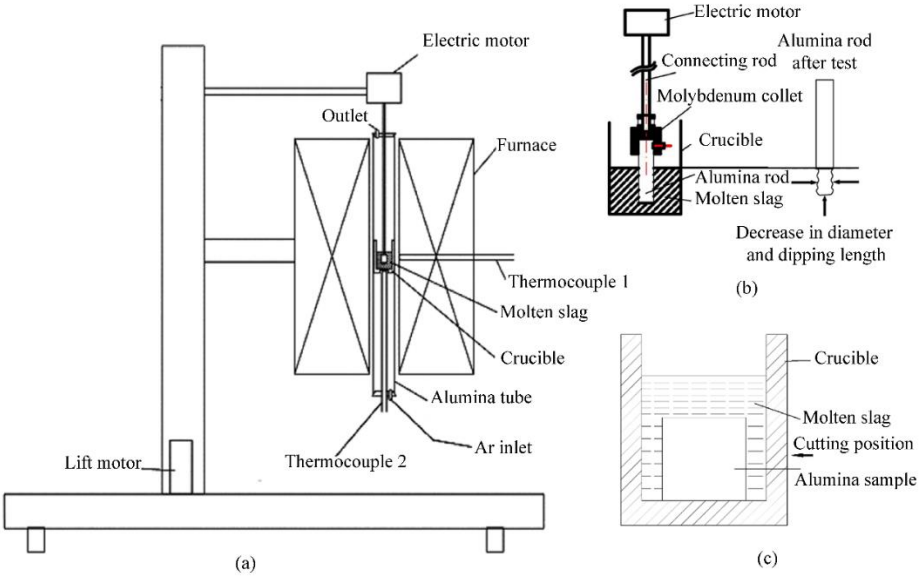

Figure 1. Schematic figure of experimental equipment and methods: (**a**) Structure diagram of Type RTW-10 melts properties analyzer; (**b**) Schematic figure of the dissolution speed experiment; (**c**) schematic figure of the static dissolution experiment.

In order to study the dissolution mechanism of alumina and the formation of intermediate compounds in the boundary layer, the static dissolution experiments were performed. Al_2O_3 rods (10 mm in diameter and 10 mm in length) were put in a graphite crucible (outer diameter 20 mm, inner diameter 15 mm, length 30 mm), then 10 g of pre-melted slag were put into the crucible. The furnace was heated to a predetermined temperature under the protection of high purity Ar gas at a flow rate of 0.5 L/min, and then thermostated for one hour. The crucible was quickly placed in the constant temperature zone of the tube furnace. Ten minutes later, the crucible was quickly taken out and cooled in the air. The Al_2O_3 rod with the solidified slag after the experiment was cut longitudinally using a diamond saw at the position shown in the Figure 1. The cross-sections were

ground and polished, then the interface between the molten slag and rod was analyzed using the scanning electronic microscopy equipped with energy dispersive spectroscopy (SEM-EDS) method. The SEM-EDS analysis was performed on an SU8010 with Bruker energy dispersed spectral, and the working voltage was 20 kV.

3. Results and Discussion

3.1. Effect of Slag Composition

In order to simultaneously ensure the reaction temperature of the self-propagating system and the flow properties of the slag, on the basis of our previous studies and phase diagram of CaO-Al_2O_3 system, a slag with w(CaO):w(Al_2O_3) = 1:2 was selected as the base slag, and the effect of CaF_2, CaO, MgO, and Na_3AlF_6 on the dissolution rates of Al_2O_3 were studied. In the experiment, the temperature was 1650 °C, the rotation speed of the rod was 200 rpm, and the rotation time was 10 min.

Macro photos of some Al_2O_3 rods are shown in Figure 2. It can be seen that both the diameter and the length decreased after the dissolution experiment. The changes in the diameter and length of the alumina rods are very different between the slags with different compositions, the size change of sample B before and after the experiment is very small, while sample C has a big change. Furthermore, the necking phenomenon was observed in some examples, this situation is caused by the Marangoni flow, which is related to the viscosity and surface tension of the melt [18]. This means that the ability of the slag to dissolve alumina can be greatly improved by changing the composition. Therefore, the measurement of the rod size needs to be repeated multiple times and then averaged.

Figure 2. Al_2O_3 rods before and after dissolution experiments: (**A**)—Original rod; (**B**)—Base slag, w(CaO):w(Al_2O_3) = 1:2; (**C**)—w(CaF_2) = 20%, w(CaO):w(Al_2O_3) = 1:2.

Figure 3a shows the effect of slag composition on the dissolution rate of Al_2O_3 at 1923 K. The effects of different kinds of additives with 5% mass fraction on viscosities and solidification temperatures are shown in Figure 3b. In Figure 3, the content of additives means that the mass fraction of the additive in the molten slag is x%, and the mass fraction of the base slag (w(CaO):w(Al_2O_3) = 1:2) is (1 − x%). It is seen in the figure that slag composition has a very significant effect on dissolution rate, and that the dissolution rate differs by several orders of magnitude. All four additives can increase the dissolution rates of Al_2O_3, and the order of influence is MgO, CaF_2, CaO, and Na_3AlF_6 from strong to weak. The additives can decrease the viscosity, but the order of influence is CaF_2, Na_3AlF_6, MgO, and CaO

from strong to weak. Surprisingly, the effect of magnesium oxide exceeds that of calcium fluoride when the addition amount is low, while the effect of cryolite on the dissolution rate is very weak, although both calcium fluoride and cryolite can greatly reduce the viscosity of the melt. This means that the dissolution rate of alumina is not only affected by the viscosity of the melt.

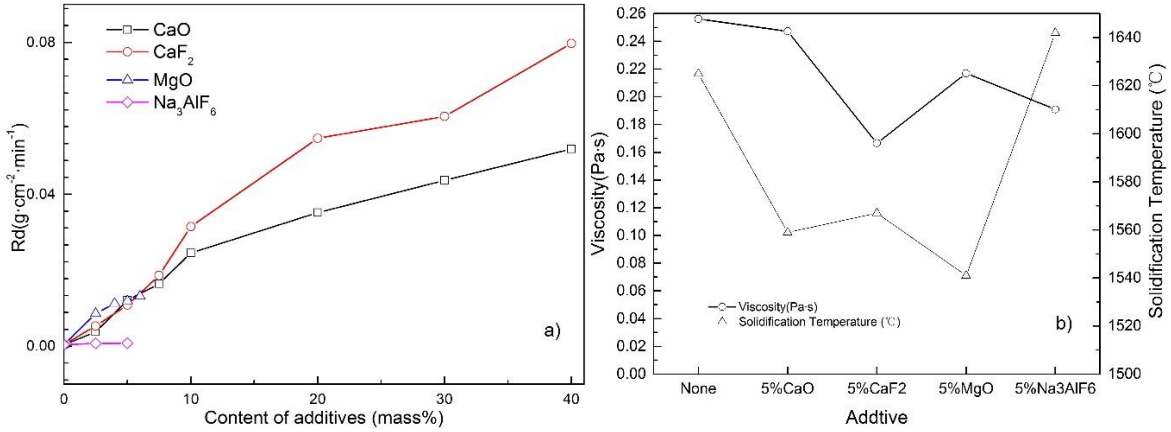

Figure 3. Effect of slag compositions on (**a**) the dissolution rate of Al_2O_3 at 1923 K (1650 °C) and (**b**) viscosities and solidification temperatures.

According to the current research results, the dissolution process of alumina in molten slag is generally affected by two aspects: mass transfer coefficient k and concentration driving force (the difference in concentration of alumina between the bulk slag and the interface) [13–15]. The influence of additives on the dissolution rate can also be explained by these two aspects. In recent years, there have been many studies on the microstructure of alumina and aluminate melts [19–22]. In the aluminate melts, it is generally considered that the coordination number of Al in the melt is 4, and the corresponding structural unit is AlO_4, and Al_2O_3 could form a network structure through Al-O-Al bonds, just like silica in silicate melts. In the pure alumina melt, AlO_4 units share oxygen ions to form a complex network structure to generate a net charge close to zero. CaO and MgO can provide free oxygen ions to the melt, while CaF_2 and Na_3AlF_6 can provide fluoride ions to the melts. After the free oxygen ions enter the melt, the tetrahedron sharing the oxygen ions is reduced to accommodate more oxygen, which will lead to the depolymerization of the melt network structure and the reduction of the size of the microstructure units. Fluoride ions also have a similar effect in the melt, and because fluoride ions cannot form Al-F-Al bonds, it is more destructive to the network structure. Therefore, all four additives can cause the depolymerization of the network structure in the melt and the reduction of the size of the microstructure unit, which is conducive to the diffusion of alumina in the melt, thereby increasing the dissolution rate of alumina. In addition, the increase of MgO, CaF_2, and CaO content can reduce the concentration of alumina in the bulk slag, thereby increasing the concentration driving force, therefore, they have a strong influence. From the relevant phase diagram [23], it can be estimated that when the content is 5% and the additives are MgO, CaO, and CaF_2, the difference in alumina content between the bulk slag and the interface slag are 8.43%, 6.17%, and 3.01%, respectively. Therefore, MgO can greatly increase the dissolution rate, although its ability to reduce the viscosity of the slag is worse than that of calcium fluoride. Na_3AlF_6 can effectively reduce the viscosity of the slag, but has little effect on the dissolution rate, which may be due to its existence reducing the driving force for mass transfer. Na_3AlF_6 contains aluminum ions, which have a low ability to reduce the alumina content in the slag. At the same time, Na_3AlF_6 will cause the solidification temperature of the melt to rise, which may be due to sodium ions causing calcium aluminate compounds with a high melting point to precipitate in the slag [24], Therefore, Na_3AlF_6 will reduce the difference in alumina concentration between the interface and the bulk slag, so its ability to increase the dissolution rate of alumina is poor.

3.2. Effect of Rotating Speed

A slag with $w(CaF_2)$ = 20%, w(CaO):w(Al_2O_3) = 1:2 was selected as the research object. The effect of rotational speed on the dissolution rate of alumina in slag was studied between 1500 and 1650 °C. The experimental results show that the dissolution rate increases significantly with the increase of the rotational speed, as shown in the Figure 4.

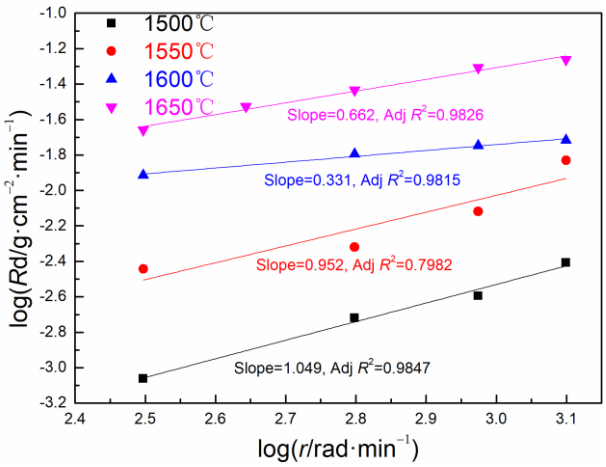

Figure 4. Effect of the rotating speed on the dissolution rate of an alumina rod.

Considering the mass balance of alumina in the dissolution process, in a unit time, the mass change of the alumina rod is equal to the alumina entering the slag, as shown in the following equation:

$$\rho_{Al_2O_3} \cdot A \cdot \left(-\frac{dr}{dt}\right) = A \cdot J_{Al_2O_3} \tag{3}$$

where A represents the contact area between the alumina rod and the slag (cm^2), $\rho_{Al_2O_3}$ represents the density of alumina rod ($g \cdot cm^{-3}$), r represents the diameter of the alumina rod(cm), and $J_{Al_2O_3}$ represents the flux of Al_2O_3 in the molten slag phase ($g \cdot cm^{-3} \cdot min^{-1}$), which could be written as Equation (4):

$$J_{Al_2O_3} = k\left(C^s_{Al_2O_3} - C^b_{Al_2O_3}\right) \tag{4}$$

where k represents the mass transfer coefficient of Al_2O_3 in the molten slag ($cm \cdot min^{-1}$) and $C^s_{Al_2O_3}$ and $C^b_{Al_2O_3}$ represent the concentrations ($g \cdot cm^{-3}$) of Al_2O_3 at the interface and in the bulk slag, respectively.

Referring to the existing research results [7–15,25], it is assumed that the rate-limiting step of the dissolution process is the diffusion of alumina in the boundary layer. Under this assumption, the mass transfer coefficient of solid oxide in the molten slag phase can be presented by the Levich equation:

$$k = 0.62 D^{2/3} v^{-1/6} \omega^{1/2} \tag{5}$$

$$R_d = 0.62 D^{2/3} v^{-1/6} \omega^{1/2} \left(C^s_{Al_2O_3} - C^b_{Al_2O_3}\right) \tag{6}$$

where D represents the diffusion coefficient of the oxide ($cm^2 \cdot min^{-1}$), v represents the kinematic viscosity of the molten slag($cm^2 \cdot min^{-1}$), and ω represents the rotational angular velocity of the alumina rod($rad \cdot min^{-1}$).

Equation (5) shows that the logarithm of the oxide dissolution rate is linearly proportional to the logarithm of the rotational speed with a slope of 0.5. In the published literature on the dissolution of alumina in slag, the slope is between 0.46 and 0.7 [10,13–15]. As shown in Figure 4, in the current study, the slope at a higher temperature (1600 and 1650 °C) is close to 0.5, but the slope is significantly

higher at lower temperatures (1500 and 1550 °C). However, a linear relationship between the logarithm of the alumina dissolution rate and the logarithm of the rotational speed at each temperature still shows strong dependence of the measured dissolution rate on the rate of rotation of the alumina rods, which will not affect diffusion in the solids. So, it can be considered that the rate-limiting step is the diffusion of Al_2O_3 in the boundary layer [7–10,25]. A higher slope shows a stronger effect of the rotational speed on the dissolution rate at lower temperatures. Since the slag used in the current study has a higher alumina concentration, its viscosity and mass transfer driving force are lower at lower temperatures, which is not conducive to the diffusion of alumina. Therefore, the rotation speed can increase the dissolution rate by improving the mass transfer conditions and exhibit a stronger influence at a lower temperature.

3.3. Effect of Temperature

Figure 5 shows the effect of temperature on the dissolution rate of alumina at different rotational speeds. The slag composition used in this section is the same as in the previous section. As can be seen from the figure, the dissolution rate of alumina increases with increasing temperature, and the natural logarithm of the dissolution rate shows a good linear relationship with the reciprocal of temperature. The increase of temperature can reduce the viscosity of the slag and accelerate the diffusion of alumina in the slag, which is beneficial to the dissolution process.

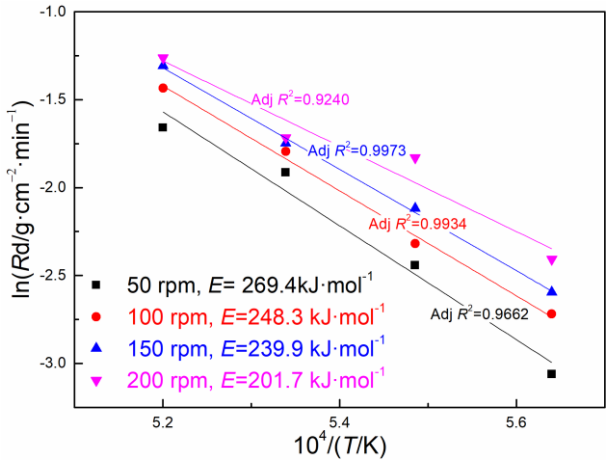

Figure 5. Effect of temperature on dissolution rate of alumina rod.

At the same time, the activation energy of the alumina dissolution process is obtained by the Arrhenius formula, as shown in Equation (7):

$$R_d = R_d^0 \exp\left(-\frac{E}{RT}\right) \tag{7}$$

where E represents the activation energy ($J \cdot mol^{-1}$), R represents the gas constant ($J \cdot mol^{-1} \cdot K^{-1}$), and T represents the thermodynamic temperature (K).

The activation energy obtained in the current study was between 201.7–269.4 $kJ \cdot mol^{-1}$, and the activation energy gradually decreased with the increase of the rotation speed. This may be due to the fact that the increase in the rotational speed favors the diffusion of alumina in the slag, thereby impairing the effect of temperature.

When the rate-limiting step of the dissolution process is the diffusion of alumina in the boundary layer, and considering that the mass transfer process in the melt is affected by the diffusion coefficient and viscosity, as written in Equation (5), The activation energy of the dissolution process can be

considered to be composed of the contribution of the diffusion coefficient and the viscosity. Therefore, the activation energy of the dissolution process can be calculated by Equation (8) [7]:

$$E = (1/6)E_\eta + (2/3)E_D \quad (8)$$

where E_η and E_D are the activation energy of viscosity and diffusivity, respectively.

The activation energy of diffusivity of alumina in slag of different compositions is usually between 240–356 kJ/mol [7]. According to our previous research, the activation energy of viscosity of the slag is about 166 kJ/mol. Therefore, it can be estimated that the activation energy of the dissolution process is between 188–265 kJ/mol, which is in good agreement with the actual measured activation energy. This result also confirms that the rate-limiting step of the dissolution process is the diffusion of alumina in the boundary layer.

3.4. Mechanism of Al_2O_3 Dissolution in Slags

When the solid oxide is in contact with the molten slag, an intermediate solid phase can be formed at the interface, and the phase will actually dissolve in the slag. Therefore, observing the interface between the alumina rod and the molten slag by a microscope will be helpful to understand the dissolution process of alumina. Much of the published literature has studied the interface phase by studying the slag layer adhered on the surface of the alumina rod after the dissolution test. In order to avoid the change of the interface when the alumina rod is taken out from the slag, this paper studied the formation of a mesophase by static dissolution experiments. The static dissolution experiments were carried out at 1650 °C with a dissolution time of 10 min. Two different components of slag were used in the experiment: slag1(w(CaO):w(Al_2O_3) = 1:2) and slag 2 (w(CaF_2) = 20%, w(CaO):w(Al_2O_3) = 1:2).

Figure 6 shows the results of the SEM-EDS analysis of the reaction interface between slag 1 and Al_2O_3. It can be seen from the SEM photograph and the elemental distribution maps that crystal grains of the intermediate compound do not appear inside the bulk slag, and the composition from the slag matrix to the inside of Al_2O_3 is excessively gentle. As shown in the line scanning results, Al and O elements increase from slag to alumina, and the fluctuation is more severe. The most obvious feature in Figure 6 is the calcium gradient in the line scan result. The Ca element decreases from slag into alumina, and two obvious platforms appear at the interface. From the calcium oxide–alumina binary phase diagram [23], it can be seen that there will be two complex oxides in the system at 1650 °C: $CaO{\cdot}2Al_2O_3$(CA2) and $CaO{\cdot}6Al_2O_3$(CA6). Therefore, it can be considered that the two platforms on the calcium content curve correspond to the two oxides CA2 and CA6, and the interface will be layered in the sequence of Al_2O_3/CA6/CA2/slag. This phenomenon means that the alumina from the corundum rod and the CaO from the molten slag counter-diffuse against each other, and alumina is not directly dissolved into the slag, but first combines with calcium oxide to form intermediate phases, and then dissolves into the slag in the form of intermediate phases.

Figure 7 shows the results of the SEM-EDS analysis of the reaction interface between slag 2 and Al_2O_3. The SEM photograph and the elemental distribution maps show that crystal grains of the intermediate compound do not appear inside the bulk slag. The F element is less distributed at the interface, and there is a significant segregation with the Ca element in some areas inside the slag. This shows that calcium fluoride does not directly participate in the interfacial reaction of the alumina dissolution process. As shown in the line scanning results, there were still two platforms for the Ca element, but on the side close to the bulk slag, the platform corresponding to $CaO{\cdot}2Al_2O_3$ becomes less noticeable. This may be due to the lower viscosity of the fluorine-containing slag 2, and faster dissolution of CA2 into the bulk slag. Therefore, the dissolution process of Al_2O_3 into slag 2 will also form two intermediate compounds $CaO{\cdot}2Al_2O_3$ and $CaO{\cdot}6Al_2O_3$. As discussed in the previous section, alumina first combines with CaO to form intermediate phases, and then dissolves into the slag in the form of intermediate phases.

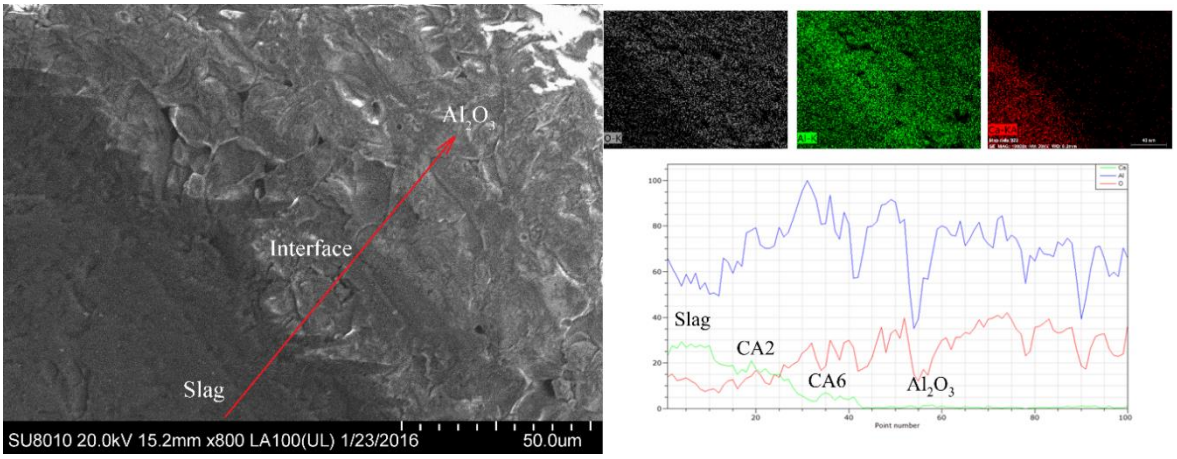

Figure 6. SEM-EDS results of the interface between Al_2O_3 and slag 1.

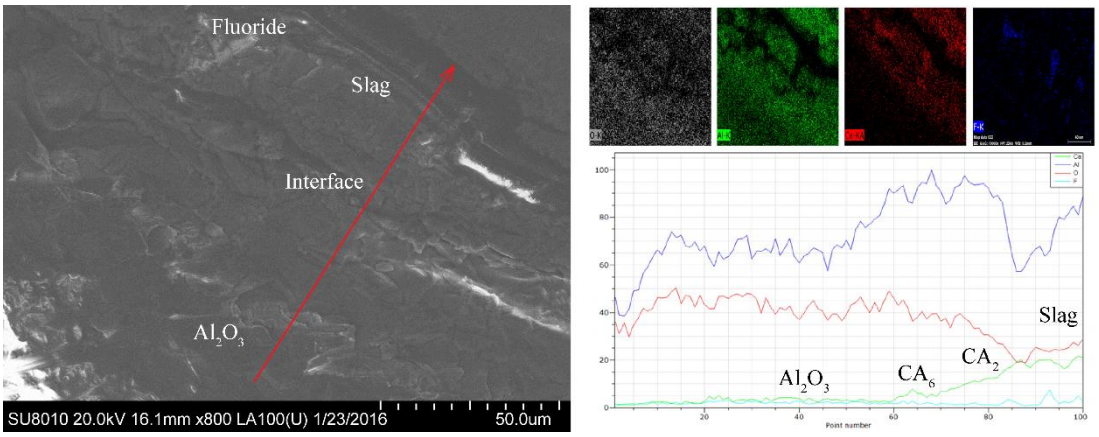

Figure 7. SEM-EDS results of the interface between Al_2O_3 and slag 2.

Based on the above research, we propose a reasonable mechanism for explaining the dissolution process of Al_2O_3 into slag, as shown in Figure 8.

In an ideal situation, the bulk slag can be considered infinite, and the dissolution of alumina will not affect its composition. At time zero, the solid alumina contacts the molten slag, CaO and Al_2O_3 begin to diffuse with each other, and a very thin transition layer with a concentration gradient of CaO and Al_2O_3 is formed at the interface. Then, immediately, the intermediate phase layers form on the side of the transition layer close to the alumina. In the two slags currently studied, the intermediate phases are $CaO{\cdot}2Al_2O_3$ and $CaO{\cdot}6Al_2O_3$. In the transition layer near the slag side, a diffusion boundary layer is formed. As time goes by, the thickness of the two intermediate phase layers and the boundary layer increases, and the diffusion fluxes of CaO and Al_2O_3 decrease and reach a "steady" state, then the interface is layered in the sequence of Al_2O_3/CA6/CA2/boundary layer/bulk slag. Therefore, in this stable state, a large flux of CaO passes through the boundary layer, and a part of it reacts with the aluminum polymer in the boundary layer, and the remaining part of the CaO reach the interface between CA2 and the boundary layer. At this interface, CA2 reacts with CaO, reaching the interface and formimg large-sized aluminum polymer melt units. Driven by the difference in concentration, these melt units move toward the bulk slag, and continuously react with CaO and depolymerize into smaller-sized aluminum polymers, and finally enter the bulk slag. Then, a smaller flow of CaO passes through the CA2 layer to the interface between the CA2 and CA6 layers, where the following reaction occurs: 2C + CA6 = 3CA2. The remaining smaller flow of CaO continues to cross the CA6 layer and when it reaches the interface between the alumina layer and CA6 layer, the following reaction occurs at this interface and CaO is finally consumed: C + 2A = CA2. Alumina passes through the CA6 layer

and the CA2 layer in turn, and reaches the interface between CA2 and the boundary layer. As a result of the foregoing discussion, the rate-limiting step of the alumina dissolution process in the slag is the diffusion of alumina in the boundary layer. Therefore, the alumina passes through the CA6 layer, the CA2 layer, and the boundary layer in sequence during the dissolution process and finally enters the bulk slag, the flow rate is determined by the rate at which the alumina passes through the boundary layer. At the same time, CaO passes through the boundary layer, the CA2 layer, and the CA6 layer, successively, and is continuously consumed, and the flow rate decreases successively, and finally CaO is consumed at the interface between the CA6 layer and the alumina. During this process, the thickness of the boundary layer and the two intermediate phase layers remain unchanged, but the position of each interface gradually moves to the inside of the alumina until the alumina is completely dissolved into the slag.

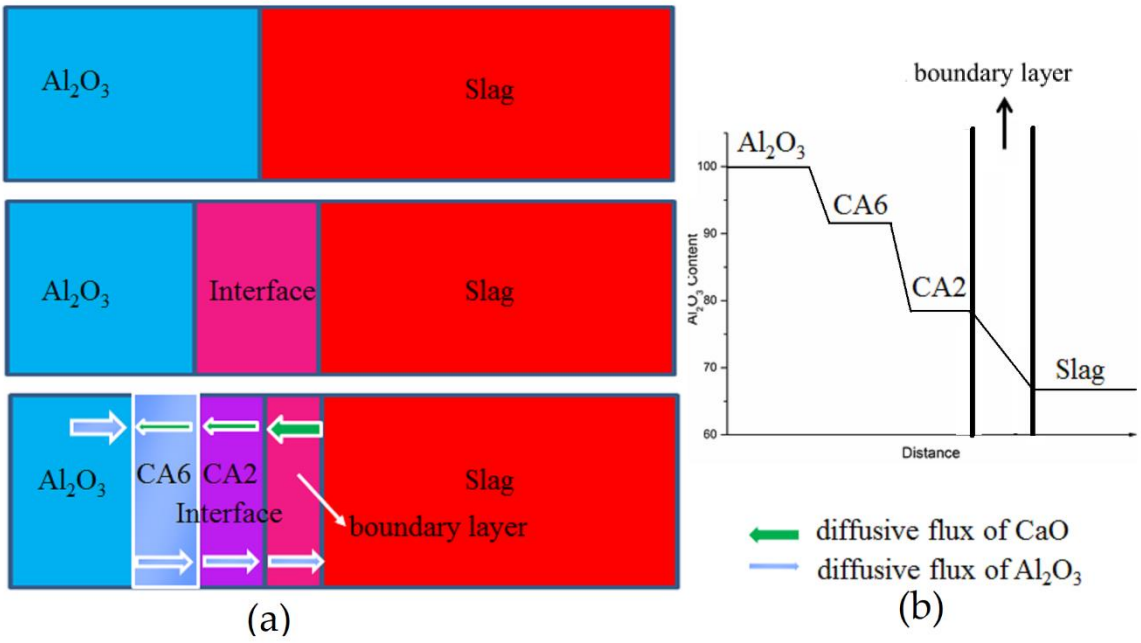

Figure 8. Schematics of (**a**) the dissolution mechanism and (**b**) concentration profile of Al_2O_3 across the interface between Al_2O_3 and slag.

4. Conclusions

Dissolution behavior of alumina in the SHS-metallurgical slag was studied using the rotating cylinder method and static dissolution experiments under an argon atmosphere. The following conclusions can be drawn:

(1) The increase of all additives can increase the dissolution rate of alumina in SHS-metallurgical slag, and the order of influence is MgO, CaF_2, CaO, and Na_3AlF_6 from strong to weak.

(2) The dissolution rate increases with increasing temperature and rotating speed. It is proposed that the rate-limiting step during the dissolution process is the diffusion of alumina in the boundary layer with formation of two intermediate phases $CaO{\cdot}2Al_2O_3$ and $CaO{\cdot}6Al_2O_3$.

(3) CaO passes through the boundary layer, the CA2 layer, and the CA6 layer in turn, and reacts with alumina to form the intermediate phases; the alumina passes through the CA6 layer, the CA2 layer, and the boundary layer in turn during the dissolution process, and finally enters the massive slag in the form of aluminum polymer.

Author Contributions: Conceptualization, G.-Y.S. and Z.-H.D.; Methodology, G.-Y.S.; Software, G.-Y.S.; Validation, Z.-H.D., G.-Y.S., and L.-P.N.; Formal Analysis, G.-Y.S.; Investigation, G.-Y.S.; Resources, T.-A.Z.; Data Curation, G.-Y.S.; Writing—Original Draft Preparation, G.-Y.S.; Writing—Review and Editing, Z.-H.D., T.-A.Z., and L.-P.N.;

Visualization, G.-Y.S.; Supervision, L.-P.N.; Project Administration, Z.-H.D.; Funding Acquisition, T.-A.Z. All authors have read and agreed to the published version of the manuscript.

Funding: This research was funded by The Open Fund Project of the Key Laboratory for Ecological Metallurgy of Multimetallic Ores (Ministry of Education), grant number NEMM2018004; The Science and Technology Research Project of the Education Department of Jiangxi Province, grant number GJJ180463; the Doctoral Scientific Research Foundation of JXUST, grant number jxxjbs17006; the National Natural Science Foundation of China, grant number 51674074, u1702253.

Conflicts of Interest: The authors declare no conflict of interest.

References

1. Si, S.H.; Zhang, H.; He, Y.Z.; Li, M.X.; Guo, S. Liquid phase separation and the aging effect on mechanical and electrical properties of laser rapidly solidified $Cu_{100-x}Cr_x$ alloys. *Metals* **2015**, *5*, 2119–2127. [CrossRef]
2. Zhang, Z.; Guo, J.; Gerhard, D.; Reinhard, P. In-situ tracking the structural and chemical evolution of nanostructured CuCr alloys. *ACTA Mater.* **2017**, *138*, 42–51. [CrossRef]
3. Dou, Z.H.; Zhang, T.A.; Yu, H.E.; Niu, L.P.; Jiang, X.L.; Yang, H. Preparation of CuCr alloys by thermit-reduction electromagnetic stirring. *J. Univ. Sci. Technol. B* **2007**, *14*, 538–542. [CrossRef]
4. Dou, Z.H.; Zhang, T.A.; Shi, G.Y.; Du, Y.J.; Niu, L.P.; Lv, G.Z.; Liu, Y.; He, J.C. Research on inclusions in CuCr alloy prepared by thermit reduction. In Proceedings of the 4th International Symposium on High-Temperature Metallurgical Processing, TMS 2013 Annual Meeting and Exhibition, San Antonio, TX, USA, 3–7 March 2013; Jiang, T., Hwang, J., Mackey, P.J., Yucel, O., Zhou, G., Eds.; John Wiley & Sons, Inc.: Hoboken, NJ, USA, 2013; pp. 247–254.
5. Dou, Z.H.; Zhang, T.A. Research progresses on the preparation of powders and alloys by SHS-metallurgy. *Mater. Chin.* **2016**, *035*, 598–605.
6. Zhang, S.W.; Hamid, R.R.; Hossain, S.; William, E.L. Alumina dissolution into silicate slag. *J. Am. Ceram. Soc.* **2000**, *83*, 897–903. [CrossRef]
7. Bui, A.H.; Ha, H.M.; Chung, I.S.; Lee, H.G. Dissolution kinetics of alumina into mold fluxes for continuous steel casting. *ISIJ Int.* **2005**, *45*, 1856–1863. [CrossRef]
8. Yu, X.; Pomfret, R.J.; Coley, K.S. Dissolution of alumina in mold fluxes. *Met. Mater. Trans. B* **1997**, *28*, 275–279. [CrossRef]
9. Susanne, M.; Jurgen, G.; Stefan, F.; Kang, Y.B.; Christian, B.; Johannes, S. Study on oxide inclusion dissolution in secondary steelmaking slags using high temperature confocal scanning laser microscopy. *Steel Res. Int.* **2016**, *87*, 57–67.
10. Xiang, S.L.; Lv, X.W.; Yu, B.; Xu, J.; Yin, J.Q. The dissolution kinetics of Al_2O_3 into molten CaO-Al_2O_3-Fe_2O_3 slag. *Met. Mater. Trans. B* **2014**, *45*, 2106–2117. [CrossRef]
11. Soll-Morris, H.; Sawyer, C.; Zhang, Z.T.; Shannon, G.N.; Nakano, J.; Sridhar, S. The interaction of spherical Al_2O_3 particles with molten Al_2O_3–CaO–FeO_x–SiO_2 slags. *Fuel* **2009**, *88*, 670–682. [CrossRef]
12. Hagemann, R.; Pettsold, L.; Sheller, P.R. The process of oxide non-metallic inclusion dissolution in slag. *Met. Min. Ind.* **2010**, *2*, 262–266.
13. Choi, J.Y.; Lee, H.G.; Kim, J.S. Dissolution rate of Al_2O_3 into molten CaO–SiO_2–Al_2O_3 slags. *ISIJ Int.* **2002**, *42*, 852–860. [CrossRef]
14. Yi, K.W.; Tse, C.; Park, J.H.; Valdez, M.; Cramb, A.W.; Sridhar, S. Determination of dissolution time of Al_2O_3 and MgO inclusions in synthetic Al_2O_3-CaO-MgO slags. *Scand. J. Met.* **2003**, *32*, 177–184. [CrossRef]
15. Li, J.L.; Shu, Q.F.; Liu, Y.A.; Chou, K.C. Dissolution rate of Al_2O_3 into molten CaO–Al_2O_3–CaF_2 flux. *Ironmak. Steelmak.* **2014**, *41*, 732–737. [CrossRef]
16. Dong, Y.; Jiang, Z.; Yu, A. Dissolution behavior of alumina-based inclusions in CaF_2-Al_2O_3-CaO-MgO-SiO_2 slag used for the electroslag metallurgy process. *Metals* **2016**, *6*, 273. [CrossRef]
17. Shi, G.Y.; Zhang, T.A.; Niu, L.P.; Dou, Z.H. The dissolution rate of solid alumina inclusion into molten CaF_2 -CaO-MgO-Al_2O_3-SiO_2 slags. In Proceedings of the 5th International Symposium on High-Temperature Metallurgical Processing, TMS 2014 Annual Meeting and Exhibition, San Diego, CA, USA, 16–20 February 2014; Jiang, T., Hwang, J., Schlesinger, M.E., Yucel, O., Padilla, R., Mackey, P.J., Zhou, G., Eds.; John Wiley & Sons, Inc.: Hoboken, NJ, USA, 2014; pp. 131–136.
18. Sun, S.; Zhang, L.; Jahanshahi, S. From viscosity and surface tension to marangoni flow in melts. *Met. Mater. Trans. B* **2003**, *34*, 517–523. [CrossRef]

19. Akola, J.; Kohara, S.; Ohara, K.; Fujiwara, A.; Watanabe, Y.; Masuno, A.; Usuki, T.; Kubo, T.; Nakahira, A.; Nitta, K.; et al. Network topology for the formation of solvated electrons in binary CaO-Al_2O_3 composition glasses. *PNAS* **2013**, *110*, 10129–10134. [CrossRef]
20. James, W.E.D.; Louis, H.; Anita, Z.; Sandro, J.; Hilip, S.S.; Daniel, R.N.; Henry, E.F. Structural transformations on vitrification in the fragile glass-forming system $CaAl_2O_4$. *Phys. Rev. Lett.* **2012**, *109*, 235501.
21. James, W.E.D.; Sandro, J.; Viviana, C.; Aleksei, B.; Marlène, L.; Séverine, B.; Henry, E.F.; Louis, H. The structure of liquid calcium aluminates as investigated using neutron and high energy x-ray diffraction in combination with molecular dynamics simulation methods. *J. Phys. Condens. Matter.* **2011**, *23*, 155101.
22. Hyun, P.J.; Min, D.J.; Song, H.S. Structural investigation of CaO-Al_2O_3 and CaO-Al_2O_3-CaF_2 slags via fourier transform infrared spectra. *ISIJ Int.* **2002**, *42*, 38–43.
23. Allibert, M. Slag atlas. In *Verein Deutscher Eisenhüttenleute*, 2nd ed.; Verlag Stahleisen: Düsseldorf, Germany, 1995; pp. 39, 349–402, 557–590.
24. Shi, G.Y.; Zhang, T.A.; Niu, L.P.; Dou, Z.H. Influence of Na_2O on properties of CaO-Al_2O_3 slag. *J. Northeast Univ. Nat. Sci.* **2012**, *33*, 1000–1003.
25. Park, Y.-J.; Cho, Y.-M.; Cha, W.-Y.; Kang, Y.-B. Dissolution kinetics of alumina in molten CaO–Al_2O_3–FetO–MgO–SiO_2 oxide representing the RH slag in steelmaking process. *J. Am. Ceram. Soc.* **2020**, *103*, 2210–2224. [CrossRef]